land

Article

Spatial-Temporal Simulation of Carbon Storage Based on Land Use in Yangtze River Delta under SSP-RCP Scenarios

Mengyao Li, Hongxia Luo *, Zili Qin and Yuanxin Tong

Chongqing Engineering Research Center for Remote Sensing Big Data Application, School of Geographical Sciences, Southwest University, Chongqing 400715, China
* Correspondence: tam_7235@swu.edu.cn

Abstract: Land use change could affect the carbon sink of terrestrial ecosystems, implying that future carbon storage could be estimated by simulating land use patterns, which is of great significance for the ecological environment. Therefore, the patterns of future land use and carbon storage under the combination scenarios of different Shared Socioeconomic Pathway (SSP) and Representative Concentration Pathway (RCP) of the Yangtze River Delta were simulated by introducing weight matrices into the Markov model and combining the PLUS and InVEST models. The results revealed that the woodland expands greatly during 2020–2060 under the SSP1-RCP2.6 scenario, and the carbon storage of 2060 is at a high level with an estimated value of 5069.31 $\times$ 10^6 t and an average annual increase of 19.13 $\times$ 10^6 t, indicating that the SSP1-RCP2.6 scenario contributes to the improvement of carbon storage. However, the area of built-up land is increasing under the SSP5-RCP8.5 scenario, and the estimated value of carbon storage is 3836.55 $\times$ 10^6 t, with an average annual decrease of 11.69 $\times$ 10^6 t, indicating that the SSP5-RCP8.5 scenario negatively affects carbon sink. Besides, the SSP2-RCP4.5 scenario causes almost no effect on land use change and carbon storage. The above results can help policymakers manage land use patterns and choose the best development scenario.

Keywords: land use; carbon storage; Markov; PLUS; InVEST

Citation: Li, M.; Luo, H.; Qin, Z.; Tong, Y. Spatial-Temporal Simulation of Carbon Storage Based on Land Use in Yangtze River Delta under SSP-RCP Scenarios. *Land* **2023**, *12*, 399. https://doi.org/10.3390/land12020399

Academic Editor: Muhammad Shafique

Received: 28 December 2022
Revised: 28 January 2023
Accepted: 29 January 2023
Published: 1 February 2023

1. Introduction

Climate warming is the primary aspect of global change, which is a significant problem for humanity in the 21st century [1,2]. According to previous studies, one of the most important strategies for dealing with global climate warming is to enhance the capacity of ecological carbon sinks to achieve carbon balance [3]. Currently, the carbon storage of terrestrial ecosystems in China is 79.2 billion tons, with woodlands accounting for about 80% of this total. Additionally, land use types such as grasslands and wetlands can improve the ecological carbon sink capacity and play a crucial role in the global carbon cycle [4,5]. Meanwhile, the carbon emissions caused by land use change account for about 14% of global carbon emissions. Thus, the change in land use types and the optimization of land use patterns can affect the carbon emission and absorption processes in the atmosphere and land by affecting the carbon storage of terrestrial ecosystems [6,7]. In the background of economic development [8,9], how to estimate future carbon storage and maintain the greatest possible carbon sink capacity of ecosystems has become an essential scientific question to be addressed at this stage [10].

The traditional methods of estimating carbon storage mainly include the vorticity correlation method [11], field survey [12], remote sensing inversion [13], and model simulation [14]. The vorticity correlation method can achieve long-term, continuous localized observations of carbon fluxes at fine time scales, such as every half hour. However, the method is inflexible at regional scales, as it is limited by the number of sites established, which is less than 100 in China [15]. Field survey can accurately estimate carbon storage, but it is hard to be used for long time series research [16] because of the large human and financial investment required for field sampling. Remote sensing inversion can access the terrestrial carbon sink capacity at the global scale in real-time. However, the spatial resolution of results is low, and atmosphere transmission models have uncertainty [17,18] for the complexity of atmospheric states. In contrast, model simulation methods are widely used because they can effectively estimate and predict carbon storage at different scales [19,20]. Currently, the InVEST model [21,22] is advantageous in simulating the pattern of carbon storage and reflecting the relationship between land use change and carbon storage due to its characteristics of less required driving data and sufficient running speed [23,24]. For instance, Gong et al. [25] and Wang et al. [26] used the InVEST model to explore the carbon storage patterns in tropical China from 2000 to 2020 and to simulate the spatial and temporal characteristics of carbon storage in the Taihang Mountains ecosystem, respectively. However, studies based on the InVEST model mainly focus on the current and past [27], but have difficulties simulating future carbon storage independently, which means that land use prediction needs to be combined.

As for land use prediction, the Cellular Automate (CA) [28] model is widely used. CA is a spatially and temporally discrete model that calculates the change probability of a cell by defining transition rules [29]. However, most studies' definition of transition rules focuses excessively on the cellular accuracy of simulation results without considering the spatial homogeneity of land use [30]. In other words, the land-use cells are treated independently in the cell-based CA. Therefore, patch-based CA was developed to simulate simultaneously land use changes of multiple adjacent homogeneous cells. For instance, Wang et al. [31] proposed a patch-based CA model that uses "patches" to represent land-use entities. Chen et al. [32] built the SA-Patch-CA model by integrating the patch-based simulation strategy with the temporal variations of urban dynamics. Liang et al. [33] integrated different planning factors into the patch-based CA model to construct the FLUS model. Lin et al. [34] proposed a landscape-driven patch-based CA (LP-CA) model by incorporating landscape pattern data. Among the patch-based CA models, a patch-generating simulation (PLUS) model [35] has advantages in terms of mining conversion rules and simulating dynamic landscape changes. The model integrates a land expansion analysis strategy and a CA model based on multi-type random patch seeds [35]. Studies [36,37] have shown that the PLUS model is more applicable than other models and provides results that are closer to actual land use patterns. However, the urban demand forecasting module of the PLUS model needs to be combined with numerical forecasting models [38], and the forecast results will affect the land use simulation accuracy. In previous studies, the system dynamic (SD) model was frequently employed for this purpose since it could take into account human activities and ecological effects [39]. However, the SD model has a complex structure and requires a large amount of socioeconomic data to fit the relationship between various components [38]. Therefore, the Markov model [40] was used for land use demand forecasting. Jenerette et al. [41] applied the Markov model to a desert landscape. The research showed that the model could reasonably replicate the land use pattern changes and obtain long-term prediction results. Still, the limitation is that the simulation results have no posteriority [42], which some scholars suggest can be overcome by introducing weights [43]. Nevertheless, there has yet to be a solution for setting the weights.

In addition, previous studies have focused on future land use changes under different development scenarios, such as the continuation of historical trends scenario, the ecological conservation scenario, and the urban development scenario [44,45]. However, a new set of scenarios with a combination of the Shared Socioeconomic Pathway (SSP) and Representative Concentration Pathway (RCP) was adopted after the launch of the 6th Coupled Model Intercomparison Project (CMIP6) in 2015 [46,47]. In view of that, the weights introduced into the Markov model need to be modified to account for different SSP-RCP scenarios. However, there has not been enough research into determining land use development weights for SSP-RCP scenarios. Therefore, a new method to define a set of objective multi-scenario weights is required to obtain more accurate land use predictions.

Based on the above analysis, the objectives of the study are: (1) to explore a set of non-subjectively defined weights introduced into the Markov and PLUS models to overcome the limitation of no posteriority and obtain the parameters under different SSP-RCP scenarios; (2) to analyze the response mechanism between land use change and carbon storage to provide policy recommendations for the region's land use restructuring and sustainable development; and (3) to obtain the spatial and temporal patterns of future land use and carbon storage in the Yangtze River Delta under different scenarios.

2. Materials and Methods

2.1. Study Area

Yangtze River Delta is located in eastern China, with geographical coordinates of 114°54′–123°10′ E and 27°2′–35°20′ N (Figure 1). According to the outline of the integrated regional development of the Yangtze River Delta, the region is officially defined as consisting of all cities in Jiangsu, Zhejiang, Anhui, and Shanghai, with a total area of over 350,000 km^2. It is one of the regions with the most active economic development in China and has a pivotal strategic position in the national modernization and overall opening pattern. However, due to high-speed economic development and rapid expansion of built-up land, woodland and cropland are decreasing year by year [48]. That is why the carbon storage in the Yangtze River Delta has changed significantly in recent years.

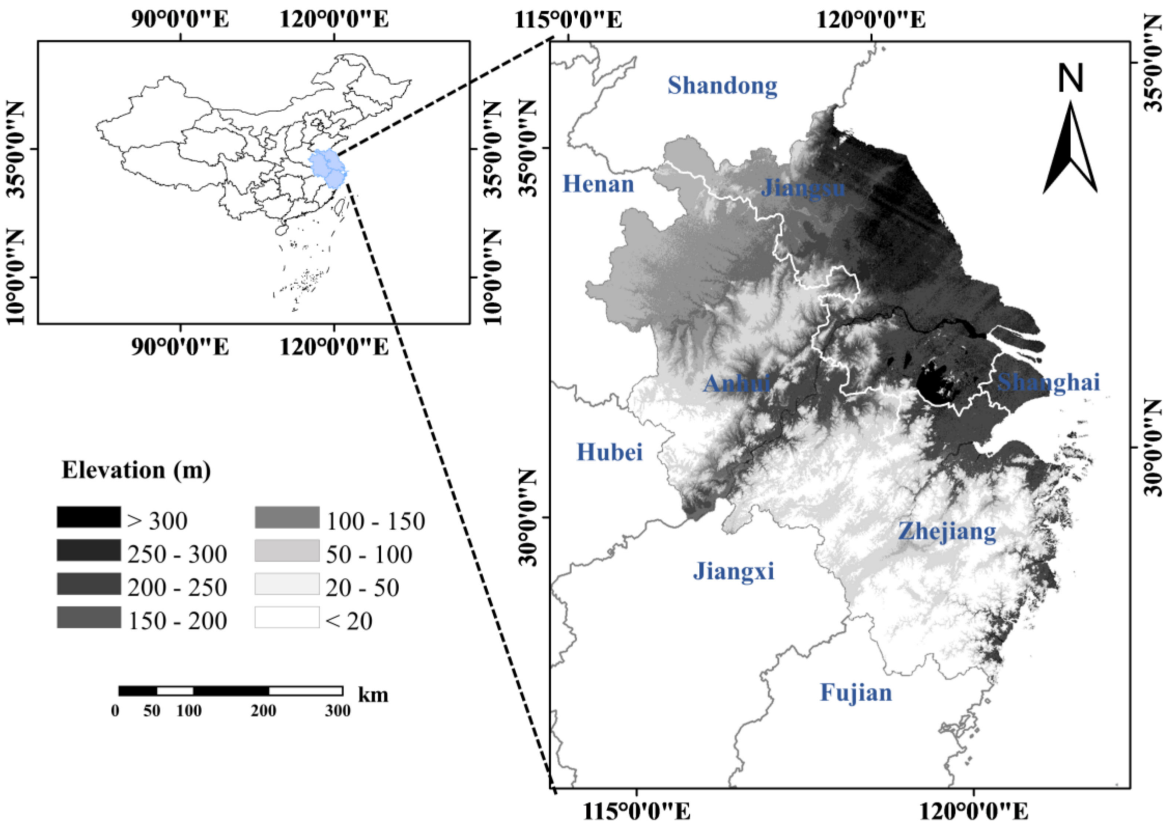

Figure 1. Geographical location of Yangtze River Delta Urban Agglomeration. (China Map from the website of China Standard Map Service (http://bzdt.ch.mnr.gov.cn/, accessed on 1 September 2022), the Map Review Number is GS (2020) 4619.

2.2. Datasets and Preprocessing

Considering the spatial resolution and data accuracy, the GlobeLand30 land use data with 30 m resolution was chosen for land use simulation. The GlobeLand30 data of 2000, 2010 and 2020 were used to obtain the transition probability, and the land use prediction was based on the data of 2000. The data of nature reserve was used as the restricted conversion boundary to avoid endless expansion of some land use types. Besides, 12 elements from meteorology, soil, socio-economics, and transportation given the previous studies were taken as driving factors [35,49–51], among which the distances to roads, railroads, and transportation stations were all Euclidean distances calculated in ArcGIS10.5 based on the corresponding vector data. The details of the data used are shown in Table 1. To avoid the incompatibility between the data, all these were converted to a raster format, and some missing raster values were filled in using neighborhood calculations. In addition, all data were standardized to 1 km resolution to obtain land use simulation results at the same resolution as theirs.

Table 1. Land use data and driving factors.

Data Type	Data Name	Resolution	Year	Data Source
Land use data	GlobeLand30 data	30 m	2000, 2010, 2020	GlobeLand30 (http://www.globallandcover.com, accessed on 16 September 2022)
Restricted conversion data	Nature reserve data	/	2018	Resource and Environment Science and Data Center (https://www.resdc.cn, accessed on 17 September 2022)
Meteorology factors	Total annual precipitation Average annual temperature	1000 m 1000 m	2000	
Soil factors	Soil type Soil erosion	1000 m 1000 m	1995	
Socio-economics factors	GDP Population	1000 m 1000 m	2000	
Terrain factors	SRTMDEMUTM 90M SRTMSLOPE 90M SRTMASPECT 90M	90 m 90 m 90 m	2000	Geospatial Data Cloud (http://www.gscloud.cn, accessed on 17 September 2022)
Transportation factors	Distance to road Distance to railroad Distance to transportation stations	/ / /	2014	OpenStreetMap (https://www.openstreetmap.org, accessed on 17 September 2022)

2.3. Method

The flowchart can be divided into three parts (Figure 2). The first part is to collect and pre-process data for analysis. Next is to calculate the multi-scenario weights and introduce them into the Markov model, from which the future land use demands are obtained. Besides, the multi-scenario land use demands are input into the PLUS model to simulate the land use patterns. Finally, the above results are combined with the carbon density data and the InVEST model, which is used to simulate the future carbon storage patterns of the Yangtze River Delta. Then the impacts of land use on them are analyzed.

2.3.1. Improved Markov Model

A Russian mathematician, Andrey Andreyevich Markov, proposed the Markov chain method in 1906. The main idea is that the current state often determines the next during the transition process of a system, which means that the method assumes that the change from one state to another is determined based on a specific transition probability. It provides a new direction for predictive probability theory [52].

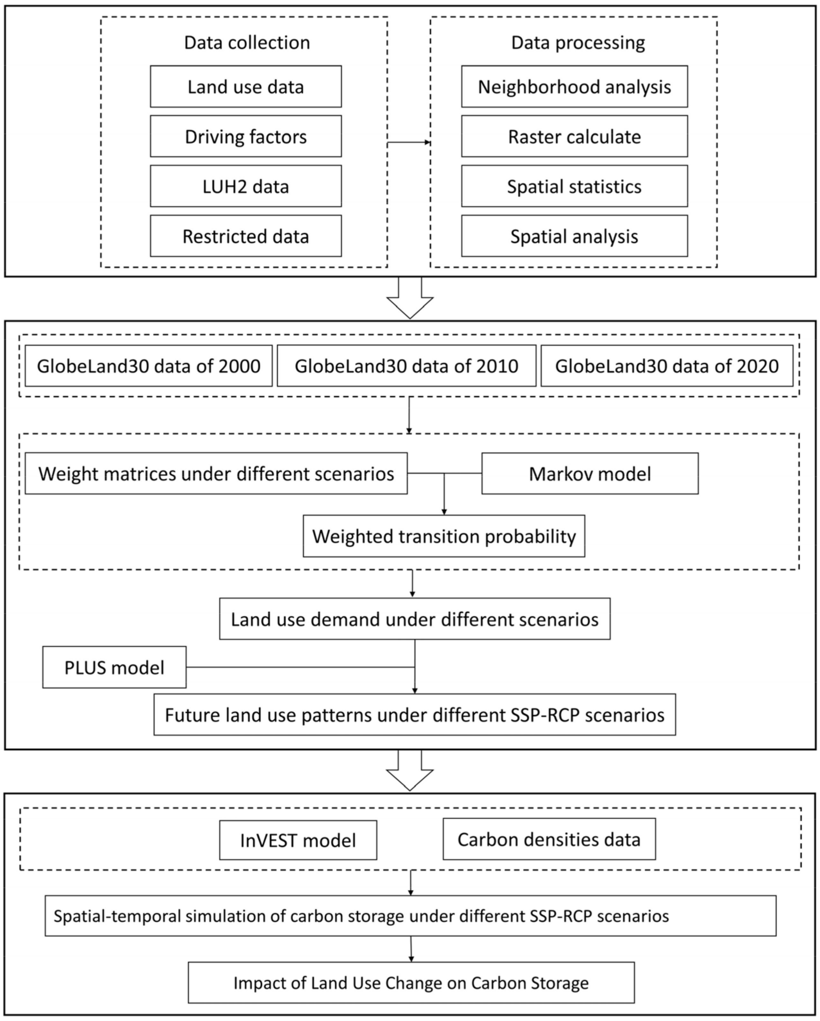

Figure 2. Methodological workflow employed in the study.

The Markov model has been widely used in various fields, including the area of land use types forecasting, where the principle is to calculate the probability matrix P_{ij} of transition by land use change within a period:

$$P_{ij} = \begin{bmatrix} P_{11} & P_{12} & \dots & P_{1n} \\ P_{21} & P_{22} & \dots & P_{2n} \\ \dots & \dots & \dots & \dots \\ P_{n1} & P_{n2} & \dots & P_{nn} \end{bmatrix} \quad (1)$$

P_{ij} represents the probability of transforming land use type from i to j in the land use change process, which takes values in the range [0, 1]; n is the total number of land use types; i, j = 1, 2, ... , n. However, the prediction results obtained by P_{ij} are deficiency of posteriority, and to address this limitation, weights w_i for land use types under different SSP-RCP scenarios are introduced to form a weight matrix W(s):

$$W(s) = \mathrm{Diag}\begin{bmatrix} w_1 & w_2 & \dots & w_n \end{bmatrix} \quad (2)$$

$$P_{ij}{}'(s) = \begin{bmatrix} P_{11} & P_{12} & \dots & P_{1n} \\ P_{21} & P_{22} & \dots & P_{2n} \\ \dots & \dots & \dots & \dots \\ P_{n1} & P_{n2} & \dots & P_{nn} \end{bmatrix} \times W(s) \quad (3)$$

$$L'(t+1) = L'(t) \times P'_{ij}(s) \tag{4}$$

$$L(t+1) = L'(t+1) / \sum_{i=1}^{n} L'_i(t+1) \tag{5}$$

$$PA = TA \times L(t+1) \tag{6}$$

where s denotes different SSP-RCP scenarios, n is the total number of land use types, and W(s) is the weight matrix of land use types in scenario s. $P_{ij}'(s)$ denotes the transition probability matrix after introducing the weight matrix in scenario s. $L'(t+1)$ and $L'(t)$ are the proportions of land use types in state t+1 and state t, respectively, and L(t+1) is the result of setting the sum of the proportions of land use types in $L'(t+1)$ to 1. PA is the predicted area of land use types, and TA is the total area.

2.3.2. The Weight Matrices of Scenarios

CMIP6 proposed a new set of scenarios with a combination of SSP and RCP, where SSP characterizes future socioeconomic development patterns and RCP characterizes future greenhouse gas emission scenarios. The representative SSP1-RCP2.6, SSP2-RCP4.5, and SSP5-RCP8.5 scenarios were chosen for the future land use simulation of the Yangtze River Delta, with the specific meanings shown in Table 2 [53].

Table 2. Future development scenario selection and description.

Scenario	Description
SSP5-RCP8.5	The future socio-economic development takes a high speed development path with large-scale use of fossil fuels, and GHG emissions are at a high level, marking the upper limit of emissions.
SSP2-RCP4.5	The future socio-economic development takes an intermediate path, with GHG emissions at a medium level.
SSP1-RCP2.6	The future socio-economic development takes a sustainable path, with GHG emissions at a low level.

The Land-Use Harmonization (LUH2) project provided a unified dataset that simulates the future land use pattern up to 2300 years under SSP-RCP scenarios, which is available for download at http://luh.umd.edu/ (accessed on 1 September 2022). However, the dataset is not easy to use directly at the scale of urban agglomeration. There are few studies based on it for the excessive spatial resolution of about 50 km. In this regard, under three SSP-RCP scenarios, the transition matrix of LUH2 data of the Yangtze River Delta during 2020–2060 was calculated. Thus, the types and areas of future land use transition were obtained, which were used to characterize the increasing and decreasing trends of land use areas. Moreover, the normalized change trends extracted from the low-resolution LUH2 data were used as weights to generate high-resolution land use data.

Nevertheless, the LUH2 dataset has a different classification system than the GlobeLand30 data, as the former has 12 land use types while the latter has only 8. For the applicability of weights, the land use types of LUH2 were reclassified as woodland, shrubland, grassland, cropland, built-up land, and bare land, making it consistent with GlobeLand30 data, as shown in Table 3.

In addition, water and wetland were assumed not to be affected by different SSP-RCP scenarios and still follow the existing transition probability, with the weights set to 1, as they were not involved in the LUH2 dataset. The weight values for all land use types under different scenarios were obtained, as shown in Table 4.

Table 3. The reclassification of land use types in LUH2.

LUH2 Land Use	Description	GlobeLand30 Land Use
primf secdf	Forested primary land Potentially forested secondary land	Woodland, shrubland
pastr range	Managed pasture Rangeland	Grassland
c3ann c3per c4ann c4per c3nfx	C3 annual crop C3 perennial crop C4 annual crop C4 perennial crop C3 nitrogen-fixing crop	Cropland
urban	Urban land	Built-up land
primn secdn	Non-forested primary land Potentially non-forested secondary land	Bare land
none	none	Water, wetland

Table 4. Weights of land use types in different scenarios.

Scenario	Cropland	Woodland	Grassland	Shrubland	Wetland	Water	Built-Up Land	Bare Land
SSP1-RCP2.6	0.89	1.14	0.92	1.14	1.00	1.00	0.90	1.01
SSP2-RCP4.5	0.98	1.09	0.77	1.09	1.00	1.00	0.95	1.13
SSP5-RCP8.5	1.14	0.95	1.05	0.95	1.00	1.00	0.99	0.93

2.3.3. PLUS Model

PLUS is a land use simulation model that integrates the LEAS (land expansion analysis strategy) and CARS (CA model based on multi-type random patch seeds) modules. The former extracts and samples the part of land use type expansion within a period and mine its driving factors by random forest algorithm. As a result, the development probability of land use types and the contribution of driving factors are obtained. Under the constraint of development probability, the CARS module combines random seed generation and threshold decreasing mechanism to obtain the land use pattern to be simulated. In addition, the confusion matrix is calculated by combing GlobeLand30 data, and the Kappa coefficient and overall accuracy are used to evaluate the simulation results.

2.3.4. InVEST Model

The InVEST model is an integrated evaluation model of ecosystem service functions and trade-offs, which aims to weigh the relationship between land use and ecosystem service functions. The carbon storage module has been widely used, which divides the carbon storage of terrestrial ecosystems into four primary carbon pools: aboveground biological carbon pool (carbon in plants surviving above the soil), belowground biological carbon pool (carbon in plant roots surviving below the soil), soil carbon pool (carbon in organic and mineral soils), and dead organic matter carbon pool (carbon in dead plants withered or standing carbon in dead plants). The total carbon storage is obtained by adding up carbon pools of each land use type, which is calculated by the following formula:

$$C_{total} = C_{total1} + C_{total2} + \ldots + C_{totaln} \quad (7)$$

$$C_{totali} = A_i \times (C_{abovei} + C_{belowi} + C_{soili} + C_{deadi}) \quad (8)$$

In the above equations, C_{total} represents the total carbon storage, C_{totali} represents the carbon storage of land use type i, and A_i represents its area. C_{abovei} represents aboveground biological carbon density, C_{belowi} represents that of belowground biological, C_{soili} represents soil carbon density, and C_{deadi} represents dead organic matter carbon density.

Therefore, the carbon densities of the four primary carbon pools of land use types are important input parameters for the InVEST model to evaluate carbon storage accurately. The carbon pool of dead organic matter is not included in the study since the carbon storage of ecosystems is little affected by it. As for the carbon densities collecting, the observation products provided by the reference carbon cycle dataset for typical Chinese forests in the National Ecosystem Science Data Center (http://www.cnern.org.cn/, accessed on 5 October 2022) were used, and carbon densities of land use types were obtained by combing previous studies [54–56]. The specific data and sources are shown in Table 5.

Table 5. Carbon density of different land use types (t/hm^2).

Land Use Type	C_{abovei}	C_{belowi}	C_{soili}
Cropland	17	80.7	108.4
Grassland	35.30	86.50	99.90
Woodland	42.40	115.90	158.80
Shrubland	5.18	8.75	151.57
Wetland	6.20	7.81	145.62
Water	0.30	0.00	0.00
Built-up land	2.50	27.5	0.00
Bare land	1.30	0.00	21.60

3. Results

3.1. Impact of Land Use Change on Carbon Storage

The carbon storage of the Yangtze River Delta was 4482.58 $\times$ 10^6 t in 2000 and 4303.96 $\times$ 10^6 t in 2020, with an average annual loss of 8.93 $\times$ 10^6 t. In the past two decades, the increase of carbon storage caused by land use change was 191.09 $\times$ 10^6 t, and the loss was 369.72 $\times$ 10^6 t.

The land use transitions that lead to carbon loss are shown in Figure 3. During the urbanization of the Yangtze River Delta, large areas of woodland, grassland and cropland were forced to be changed to built-up land with negligible carbon storage, resulting in carbon storage loss. The amount of carbon loss due to the transition from cropland to built-up land in the Yangtze River Delta between 2000 and 2020 is 170.30 $\times$ 10^6 t, accounting for the highest percentage of carbon loss at 46.06%. That is mainly because the transition area far exceeds others, which implies that the main reason for the decrease in carbon storage in the Yangtze River Delta is that urban expansion has occupied a large amount of cropland during the past 20 years.

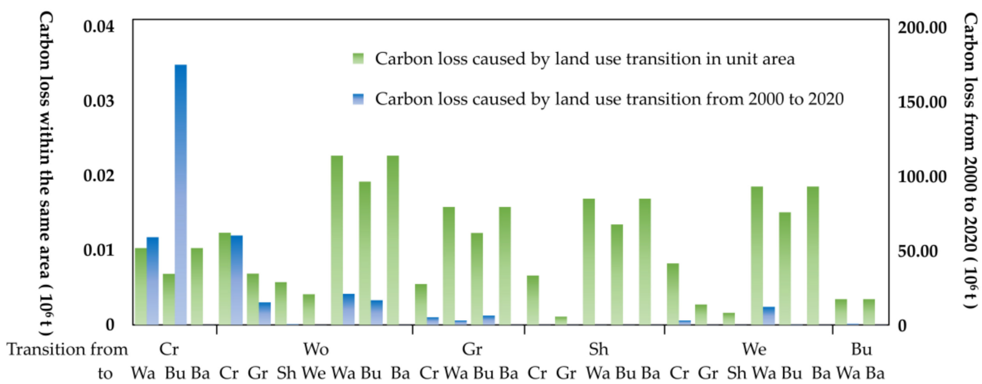

Figure 3. Carbon storage loss caused by land use change. Cr: cropland; Wo: woodland; Gr: grassland; Sh: shrubland; We: wetland; Bu: built-up land; Wa: water; Ba: bare land.

As shown in Figure 4, the areas of high carbon loss during 2000–2020 are mainly concentrated in the south and west. As can be seen from Figure 5, the main reason for the above phenomenon is that woodland is occupied by built-up land. That demonstrates that the transition of woodland during the past 20 years is also an important cause of carbon loss. As for the east and the north, the carbon loss is at a medium or low level, widely distributed and patchy, and this is caused mainly by the transition of cropland to built-up land. In addition, carbon loss showed an apparent spatial heterogeneity, indicating that the economic growth rate and local policies in different regions will significantly affect carbon storage through land use changes.

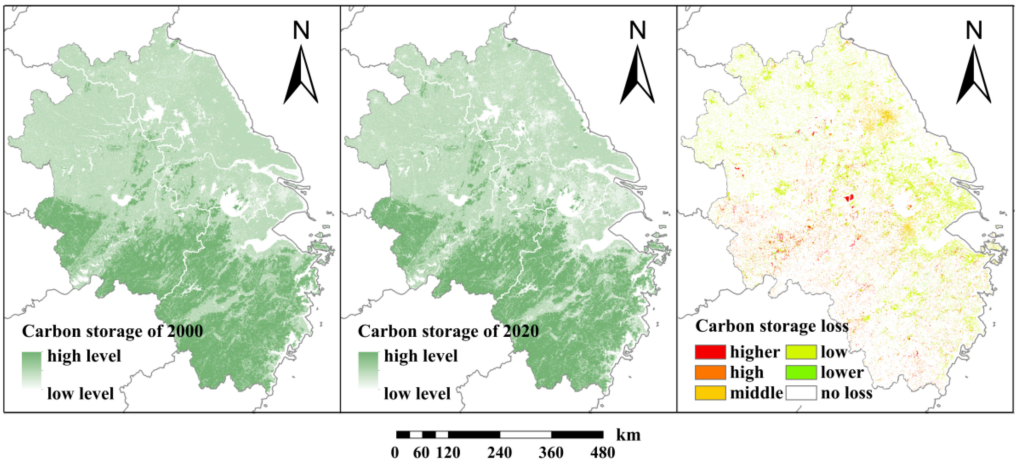

Figure 4. Patterns of carbon storage and loss in Yangtze River Delta from 2000 to 2020.

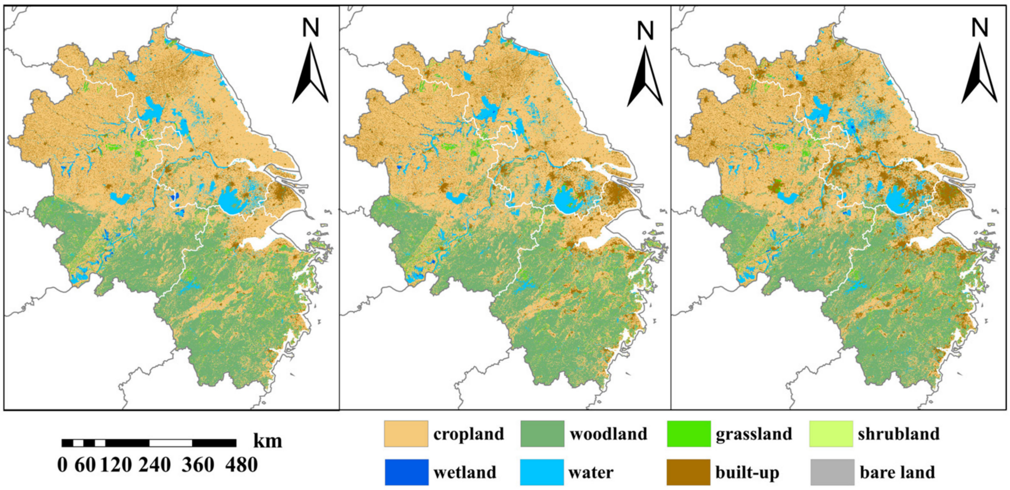

(**a**) (**b**) (**c**)

Figure 5. Land use patterns: (**a**) land use pattern of 2000, (**b**) land use pattern of 2010, (**c**) land use pattern of 2020.

3.2. Assessment of Land Use Simulation Model Results

3.2.1. Forecast of Land Use Area for the Yangtze River Delta under Different Scenarios

The area of land use types in 2010 and 2020 was forecasted by the Markov model based on the land use data of 2000, and GlobeLand30 data evaluated the accuracy of the result. As shown in Figure 6, the relative error of Markov's 2010 simulation results is 24.05% for wetlands, 12.67% for built-up land, and below 10.00% for all other land use types. As for the simulation results of 2020, the relative error is 5.73% for wetlands, 3.67% for bare land, and the relative errors of other land use types are below 1.00%, which indicates that the Markov model can forecast the future land use area well in general.

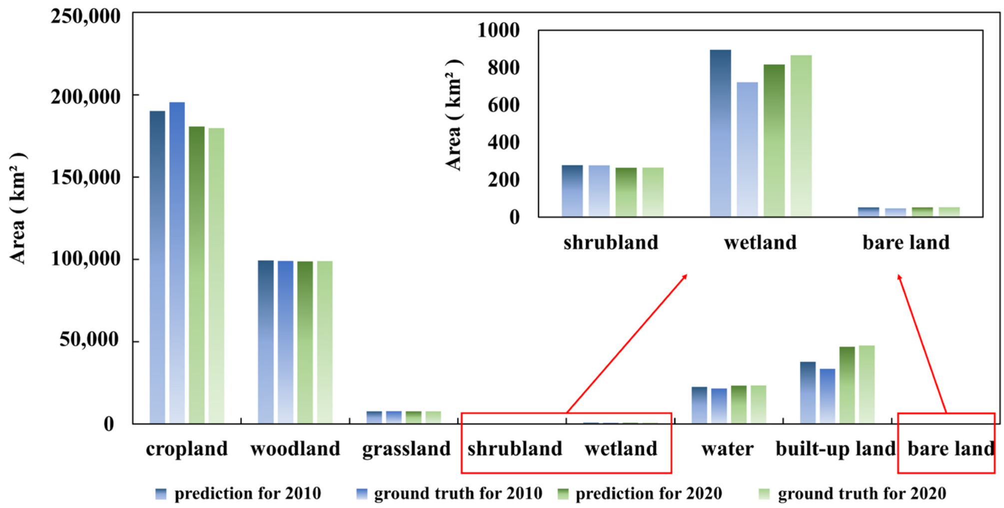

Figure 6. Comparison of land use simulation of Markov with existing data.

Figure 7 shows the results of the Markov model for land use area forecasting in 2030, 2040, 2050, and 2060 for the Yangtze River Delta under different SSP-RCP scenarios. It is observed that the cropland area slowly decreases under the SSP1-RCP2.6 and SSP2-RCP4.5 scenarios and increases under the SSP5-RCP8.5 scenario in the future 40 years, while the area of woodland and shrubland only decreases under the SSP5-RCP8.5 scenario. In addition, the area of built-up land tends to increase in the early stage and decrease in the later stage under the SSP1-RCP2.6 scenario, increasing slowly until stable under the SSP2-RCP4.5 scenario when expanding continuously under the SSP5-RCP8.5 scenario. Besides, the remaining land use types are mostly the same due to their small area share.

3.2.2. Simulation of Land Use Patterns for the Yangtze River Delta under Different Scenarios

Taking the results of the Markov model as input parameters, the PLUS model was used to simulate the land use patterns in 2010 and 2020, and the GlobeLand30 data were used to evaluate the simulation accuracy. As shown in Figure 8, the simulated results of the PLUS model in 2010 and 2020 are highly spatially consistent with the actual land use pattern, and the overall accuracy and Kappa coefficient are shown in Table 6. There is no doubt that the PLUS model can better simulate the future land use pattern.

Table 6. The accuracy assessment of PLUS model.

	2010	**2020**
Overall accuracy	0.90	0.85
Kappa coefficient	0.84	0.77

Figure 9 shows the simulations of land use patterns in 2030, 2040, 2050, and 2060 for the Yangtze River Delta under different SSP-RCP scenarios. It can be observed that the woodland tends to gradually expand to the surroundings under the SSP1-RCP2.6 scenario, with the area of built-up land in a decreasing trend, while under the SSP5-RCP8.5 scenario, the woodland gradually changes from patchy distribution to sporadic distribution, and the built-up land keeps expanding to the outside. The spatial change of land use is negligible in the SSP2-RCP4.5 scenario.

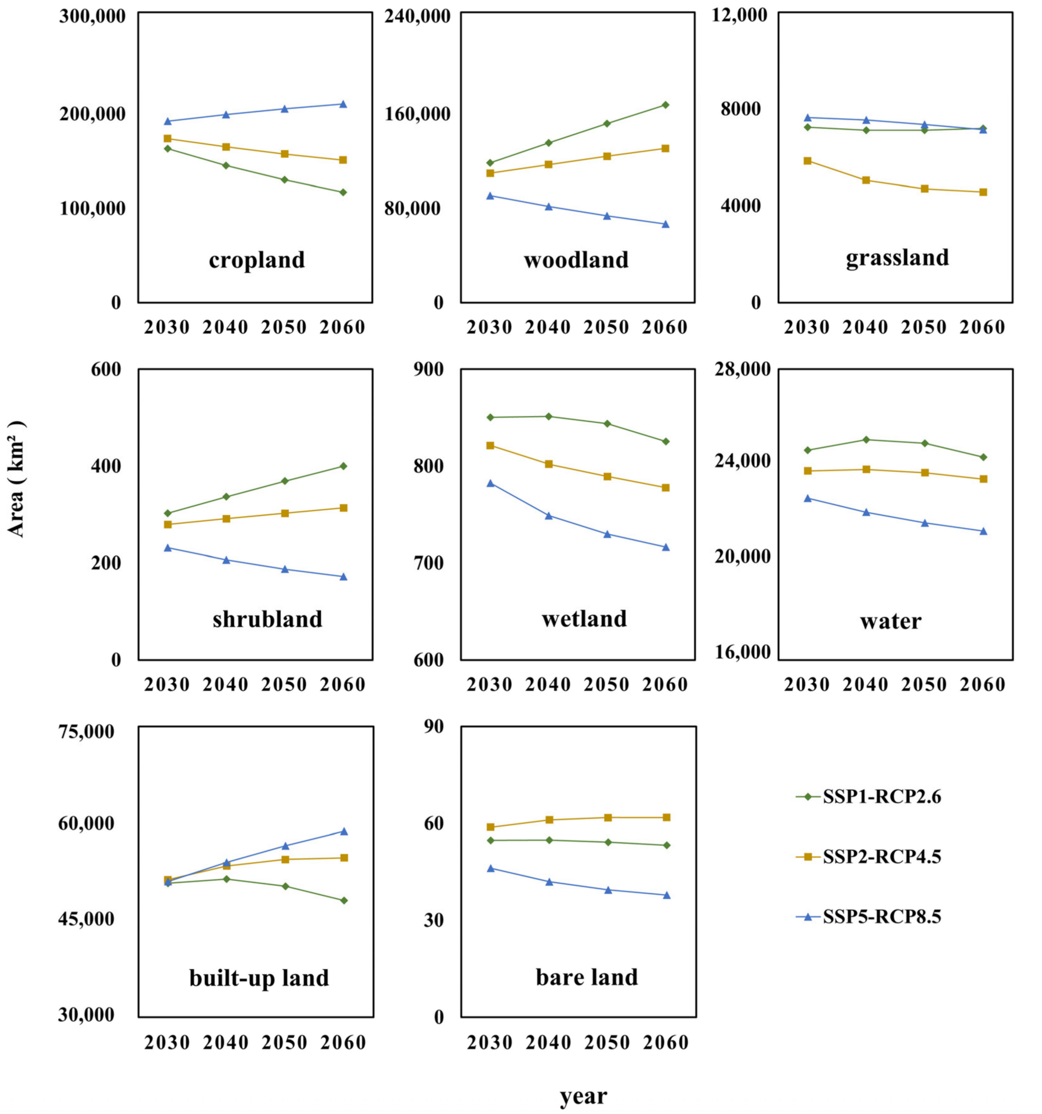

Figure 7. Forecast of land use area under different scenarios in the Yangtze River Delta of 2030, 2040, 2050, 2060.

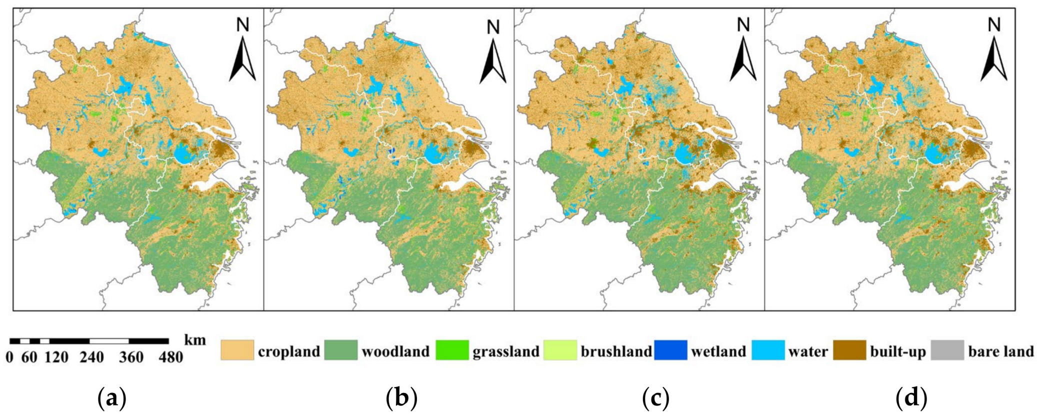

Figure 8. Comparison between simulated land use patterns and Globeland30 data: (**a**) GlobeLand30 of 2010, (**b**) simulated land use of 2010, (**c**) GlobeLand30 of 2020, (**d**) simulated land use of 2020.

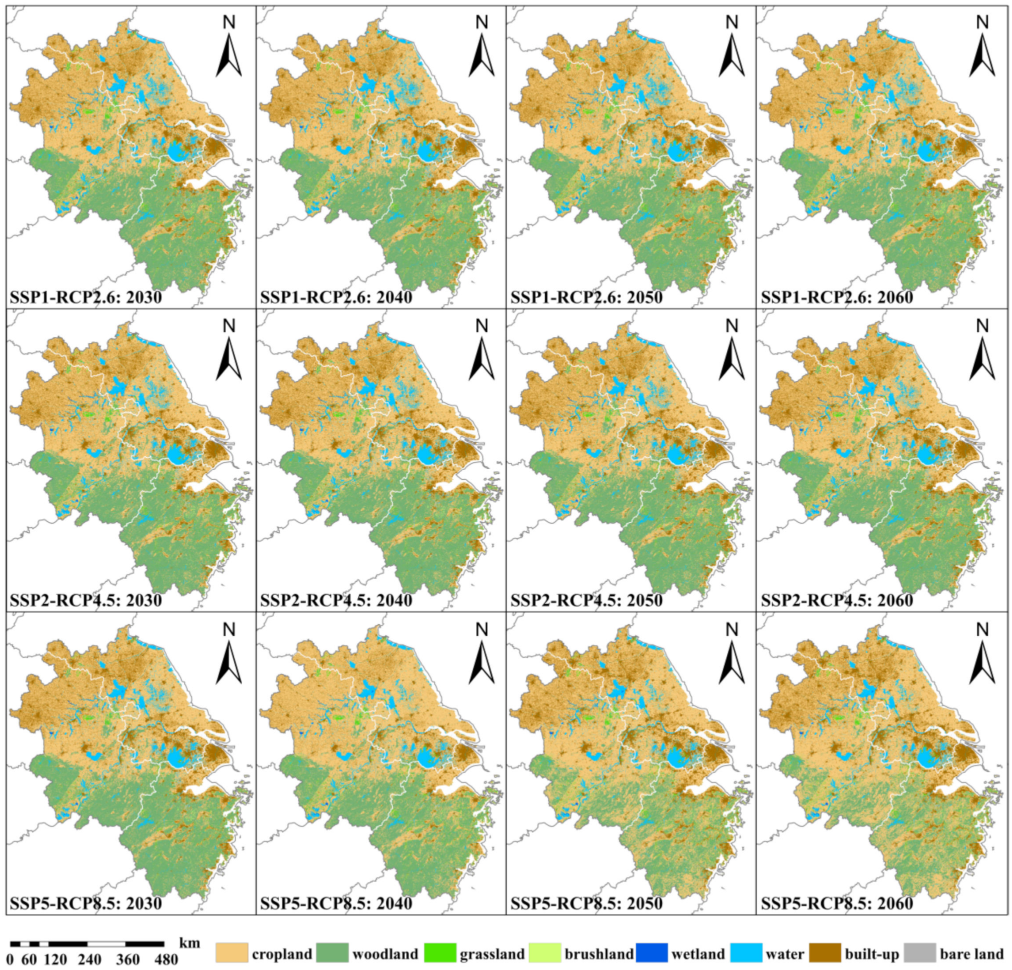

Figure 9. Simulation of land use patterns under different scenarios of 2030, 2040, 2050, 2060.

3.3. Future Carbon Storage Pattern in the Yangtze River Delta under Different Scenarios

The carbon storage patterns under different SSP-RCP scenarios in 2030, 2040, 2050, and 2060 are shown in Figure 10. The area with high carbon storage is the south of the Yangtze River Delta, with satisfactory vegetation cover and strong carbon fixation capacity. As can be seen from Figure 10, the high carbon storage area under the SSP1-RCP2.6 scenario is expanding, while that under the SSP5-RCP8.5 scenario is decreasing. In addition, the estimated carbon storage in 2060 is 5069.31 $\times$ 10^6 t and 3836.55 $\times$ 10^6 for the two, respectively, with the former increasing by 19.13 $\times$ 10^6 t per year and the latter decreasing by 11.69 $\times$ 10^6 t per year. Besides, there is not much change in the area of high carbon storage at the SSP2-RCP4.5 scenario, with an estimated carbon storage of 4583.17 $\times$ 10^6 t in 2060 and an average increase of 6.98 $\times$ 10^6 t per year.

As shown in Figure 11, the area of carbon loss under the SSP5-RCP8.5 scenario accounts for 16.79% of the total area, with a loss of 599.67 $\times$ 10^6 t during 2020–2060. In addition, the area with high carbon loss is mainly located within the woodland in the southern part of the Yangtze River Delta. In contrast, the area share, and the amount of carbon loss under the SSP1-RCP2.6 and SSP2-RCP4.5 scenarios are 1.18%, 38.70 $\times$ 10^6 t, 2.13%, and 60.64 $\times$ 10^6 t, respectively, which are much lower than those under the SSP5-RCP8.5 scenario.

Figure 10. Carbon storage patterns under different scenarios of 2030, 2040, 2050, 2060.

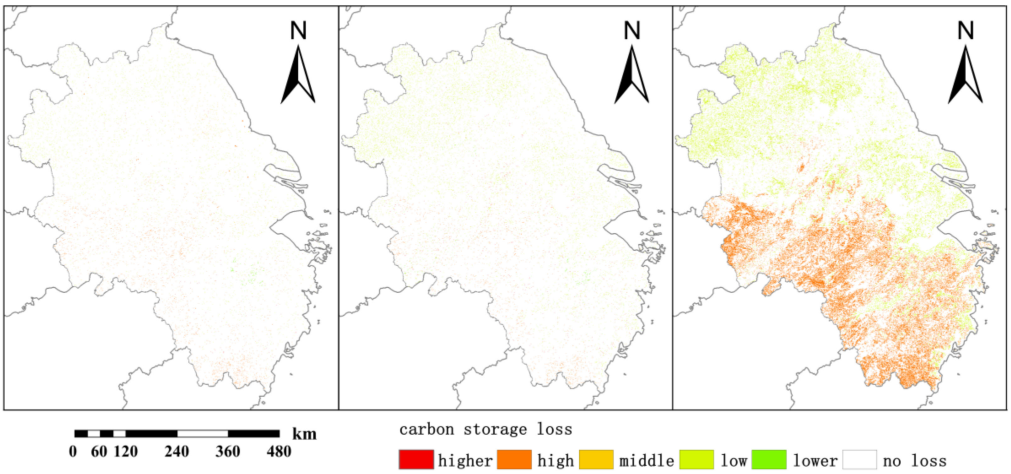

Figure 11. Carbon storage loss during 2020–2060 under different scenarios.

4. Discussion

4.1. Advantages of Introducing Multi-Scenario Weight Matrices

Numerical-spatial model integration could reveal the complex land use change process [57], which is the mainstream land use simulation method. By numericalizing

LUH2 data as weights for land use types under different SSP-RCP scenarios, the limitation that low-resolution data cannot be applied to an urban scale [58,59] is overcome. Besides, introducing multi-scenario weights allows the Markov model to overcome the drawback of no posteriority and makes it applicable to different SSP-RCP scenarios [43], which can provide input parameters for the PLUS model. Besides, the prediction accuracy shows that the Markov and PLUS models perform satisfactorily, indicating that the integration is suitable for area forecasting and pattern simulation of land use types.

4.2. Impact of Land Use Change on Carbon Storage

The changes in land use types cause different impacts on carbon storage due to the land use transition and carbon density differences [25]. Specifically, the expansion of built-up land will weaken the carbon sink capacity of the ecosystem [60,61]. Meanwhile, forest carbon is the most significant carbon pool of terrestrial ecosystems [62,63], which means that afforestation and woodland restoration have a positive impact on carbon storage [64]. However, due to the rapid economic development of the Yangtze River Delta, more or less built-up land inevitably occupies cropland and woodland to build towns and accommodate the non-native population [65]. Under the guidance of a series of environmental protection policies, such as returning cropland to woodland, the impact of woodland occupation by built-up land has been reduced to some extent [66]. That makes urban expansion due to the transition of cropland gradually becoming the main threat of carbon loss. Hence, the transition of cropland and woodland needs to be taken seriously in light of current trends.

Given the results section, carbon storage under the SSP1-RCP2.6 and SSP2-RCP4.5 scenarios develops in a positive trend, while it deteriorates gradually under the SSP5-RCP8.5 scenario. This trend implies that the SSP1-RCP2.6 scenario can effectively enhance the carbon sink capacity of ecosystems and promote carbon cycling to achieve the carbon neutrality target as early as possible [67]. However, it takes more time to achieve carbon neutrality under the SSP2-RCP4.5 scenario. Moreover, under the SSP5-RCP8.5 scenario, it is challenging to improve carbon storage and may even negatively impact the ecological environment. Therefore, measures are required to prevent the SSP5-RCP8.5 scenario. In this regard, the macroeconomic regulation of the government plays an important role [51]. It is imperative to provide policy guidance and restrictions on urban construction [68], such as strictly following the permanent basic farmland protection red line, ecological conservation red line, and urban development boundary line. Furthermore, attention should be paid to the allocation of green infrastructure and the efficient use of land, both of which are crucial for ecological environment protection.

4.3. Limitation

The improved Markov model and PLUS model simulated future land use patterns under different SSP-RCP scenarios; however, this study is limited in a few aspects. First, the simulation has yet to consider future policy interventions, such as the constrained and planned development zones designated in the future. These new policy interventions will be continuously considered in future work to establish a more complete land use prediction system. Second, the carbon densities used in the InVEST model were obtained by reviewing previous literature. However, this approach ignores the change in carbon density over time for the same land type. Finally, the GlobeLand30 is global scale data [69], and there is no doubt that field survey data can improve the accuracy of land use simulation. However, the assessment of GlobeLand30 data from previous studies showed satisfactory accuracy at the provincial scale in China [69–71]. Besides, the field survey workload is relatively large for the Yangtze River Delta. For all these reasons, GlobeLand30 data is not a bad choice.

5. Conclusions

By introducing the scenario weight matrices, the future patterns of land use and carbon storage of the Yangtze River Delta under different SSP-RCP scenarios were simulated, and the variation characteristics were analyzed. The following conclusions were obtained:

(1) The improved Markov-PLUS integrated model provides satisfactory land use prediction accuracy. The maximum relative error of 24.05% is achieved in area forecasting, and overall accuracy in spatial pattern simulation is 0.85–0.90 with kappa coefficients of 0.77–0.84. The series validation accuracy indicates that the integrated model is applicable to area forecast and spatial pattern simulation of land use types.
(2) Under the SSP1-RCP2.6 scenario, the woodland area in the Yangtze River Delta expands significantly, and the carbon storage in 2060 is estimated to be 5069.31 $\times 10^6$ t, with an average annual increase of 19.13 $\times 10^6$ t compared to 2020. Under the SSP2-RCP4.5 scenario, the land use changes little, and the estimated value is 4583.17 $\times 10^6$ t, with an average annual increase of 6.98 $\times 10^6$ t. However, the built-up land expands more under the SSP5-RCP8.5 scenario, and the estimated carbon storage of 2060 is 3836.55 $\times 10^6$ t, with an average decrease of 11.69 $\times 10^6$ t per year.
(3) The SSP1-RCP2.6 scenario causes a facilitating effect on enhancing the carbon sink capacity of ecosystems, and the SSP2-RCP4.5 scenario has a negligible effect, while the SSP5-RCP8.5 scenario causes a negative effect. Thus, policymakers should design land use policies and urban development plans according to local conditions so that the SSP5-RCP8.5 scenario should not come. Only then can the carbon storage of ecosystems be increased, and the goal of co-development of economy and ecology be achieved.

In addition, future research will explore the following aspects in depth:

- Policy implications will be taken into account.
- The temporal trends of carbon density will be explored to improve the accuracy of carbon density estimation.
- Land use data with higher accuracy will be applied to the study to obtain more realistic simulation results.

Author Contributions: Conceptualization, M.L.; methodology, M.L.; software, M.L.; validation, M.L.; formal analysis, M.L.; investigation, H.L.; resources, H.L.; data curation, H.L.; writing—original draft preparation, M.L.; writing—review and editing, M.L.; visualization, Z.Q.; supervision, Z.Q.; project administration, Y.T.; funding acquisition, Y.T. All authors have read and agreed to the published version of the manuscript.

Funding: This research was funded by the Project of Innovative Talents Training in Primary and Secondary Schools in Chongqing: The Eagle Project of Chongqing Education Commission, grant number CY210230.

Data Availability Statement: The data presented in this study are available on request from the corresponding author.

Acknowledgments: We thank the ArcGIS software for providing us with a computing platform and the European Space Agency for providing us with free data. We also thank anonymous reviewers for their insightful advice.

Conflicts of Interest: The authors declare no conflict of interest.

References

1. Lü, W.W.; Ren, H.Y.; Ding, W.C.; Li, H.; Yao, X.; Jiang, X. The effects of climate warming on microbe-mediated mechanisms of sediment carbon emission. *J. Environ. Sci.* **2023**, *129*, 16–29. [CrossRef]
2. Neupane, A.; Lazicki, P.; Mayes, M.A.; Lee, J.; Jagadamma, S. The use of stable carbon isotopes to decipher global change effects on soil organic carbon: Present status, limitations, and future prospects. *Biogeochemistry* **2022**, *160*, 315–354. [CrossRef]
3. Friedlingstein, P.; O'Sullivan, M.; Jones, M.W.; Andrew, R.M.; Hauck, J.; Olsen, A.; Peters, G.P.; Peters, W.; Pongratz, J.; Sitch, S.; et al. Global Carbon Budget 2020. *Earth Syst. Sci. Data* **2020**, *12*, 3269–3340. [CrossRef]
4. Li, H.Y.; Qu, Y.; Zeng, X.Y.; Zhang, H.Q.; Cui, L.; Luo, C.Y. Dynamic response of the vegetation carbon storage in the sanjiang plain to changes in land use/cover and climate. *Herit. Sci.* **2021**, *9*, 134–146. [CrossRef]
5. Piao, S.; Fang, J.; Ciais, P.; Peylin, P.; Huang, Y.; Sitch, S.; Wang, T. The carbon balance of terrestrial ecosystems in China. *Nature* **2009**, *458*, 1009–1013. [CrossRef]
6. Huang, X.J.; Zhang, A.L.; Zhao, R.Q.; Gao, F.; Zhang, H.H. Carbon Emission Peak, Carbon Neutrality and Territorial Spatial Planning Implementation Mechanism. *Mod. Urban Res.* **2022**, *1*, 1–5.

7. Liao, W.L.; Liu, X.P.; Xu, X.Y.; Chen, G.Z.; Liang, X.; Zhang, H.H.; Li, X. Projections of land use changes under the plant functional type classification in different SSP-RCP scenarios in China. *Sci. Bull.* **2020**, *65*, 1935–1947. [CrossRef]
8. Li, J.; Gong, J.; Guldmann, J.M.; Yang, J.; Zhang, Z. Simulation of Land-Use Spatiotemporal Changes under Ecological Quality Constraints: The Case of the Wuhan Urban Agglomeration Area, China, over 2020–2030. *Int. J. Environ. Res. Public Health* **2022**, *19*, 6905. [CrossRef]
9. Li, Z.J. Calculation of Terrestrial Carbon Sink Capacity in Dongying City, Shandong Province. *Adv. Mater. Res.* **2013**, *2482*, 1901–1904. [CrossRef]
10. Liu, W.; Qin, B. Low-carbon city initiatives in China: A review from the policy paradigm perspective. *Cities* **2016**, *51*, 131–138. [CrossRef]
11. He, H.L.; Yu, G.R.; Zhang, L.M.; Sun, X.M.; Su, W. Simulating CO_2 flux of three different ecosystems in ChinaFLUX based on artificial neural networks. *Sci. China Ser. D* **2006**, *49*, 252–261. [CrossRef]
12. Wang, G.C. A View on Measurement Methods for Greenhouse Gases Emission from Terrestrial Ecosystem. *Clim. Environ. Res.* **1997**, *2*, 251–263.
13. Wu, H.; Xu, H. Research Progress in Estimating Carbon Storage of Forest Ecosystem. *For. Resour. Manag.* **2021**, *6*, 43–51. [CrossRef]
14. Fang, J.Y.; Guo, Z.D.; Piao, S.L.; Chen, A.P. Terrestrial vegetation carbon sinks in China, 1981–2000. *Sci. China Ser. D* **2007**, *50*, 1341–1350. [CrossRef]
15. Zhao, L.; Yin, M.F.; Chen, X.F.; Wang, D.Q. Summary of the Research Methods of Forest Carbon Sink Accounting. *J. Northwest For. Univ.* **2008**, *23*, 59–63.
16. Filipchuk, A.; Moiseev, B.; Malysheva, N.; Strakhov, V. Russian forests: A new approach to the assessment of carbon stocks and sequestration capacity. *Environ. Dev.* **2018**, *26*, 68–75. [CrossRef]
17. Schedlbauer, J.L.; Polohovich, S. Current and Future Carbon Storage Capacity a Southeastern Pennsylvania Forest. *Nat. Areas J.* **2020**, *40*, 300–308. [CrossRef]
18. Lipatov, D.N.; Shcheglov, A.I.; Manakhov, D.V.; Brekhov, P.T. Spatial Variation of Organic Carbon Stocks in Peat Soils and Gleyzems in the Northeast of Sakhalin Island. *Eurasian Soil Sci.* **2021**, *54*, 226–237. [CrossRef]
19. Ma, W.S.; Wu, T.H.; Wu, X.D.; Yue, G.Y.; Li, R.; Li, X.F.; Zhu, X.F.; Hu, G.J.; Qiao, Y.P.; Hao, J.M.; et al. Warming could shift steppes to carbon sinks and meadows to carbon sources in permafrost regions: Evidence from the improved IBIS model. *Catena* **2021**, *200*, 105168–105179. [CrossRef]
20. Liu, C.; Liang, Y.; Zhao, Y.J.; Liu, S.S.; Huang, C.B. Simulation and Analysis of the Effects of Land Use and Climate Change on Carbon Dynamics in the Wuhan City Circle Area. *Int. J. Environ. Res. Public Health* **2021**, *18*, 11617. [CrossRef]
21. Nelson, E.; Mendoza, G.; Regetz, J.; Polasky, S.; Tallis, H.; Cameron, D.R.; Chan, K.M.A.; Daily, G.C.; Goldstein, J.; Kareiva, P.M.; et al. Modeling multiple ecosystem services, biodiversity conservation, commodity production, and tradeoffs at landscape scales. *Front. Ecol. Environ.* **2009**, *7*, 4–11. [CrossRef]
22. Nemec, K.T.; Raudsepp-Hearne, C. The use of geographic information systems to map and assess ecosystem services. *Biodivers. Conserv.* **2012**, *22*, 1–15. [CrossRef]
23. Lin, B.Q.; Ma, R.Y. Towards carbon neutrality: The role of different paths of technological progress in mitigating China's CO_2 emissions. *Sci. Total Environ.* **2021**, *813*, 152588. [CrossRef] [PubMed]
24. Sheikh, M.A.; Tiwari, A.; Anjum, J.; Sharma, S. Dynamics of carbon storage and status of standing vegetation in temperate coniferous forest ecosystem of north western Himalaya India. *Vegetos* **2021**, *34*, 822–833. [CrossRef]
25. Gong, W.F.; Duan, X.Y.; Mao, M.J.; Hu, J.H.; Sun, Y.X.; Wu, G.H.; Zhang, Y.Y.; Xie, Y.D.; Qiu, X.C.; Rao, X.D.; et al. Assessing the impact of land use and changes in land cover related to carbon storage by linking trajectory analysis and InVEST models in the Nandu River Basin on Hainan Island in China. *Front. Environ. Sci.* **2022**, *10*, 1038752. [CrossRef]
26. Wang, C.W.; Luo, J.J.; Qing, F.; Tang, Y.; Wang, Y.F. Analysis of the Driving Force of Spatial and Temporal Differentiation of Carbon Storage in Taihang Mountains Based on InVEST Model. *Appl. Sci.* **2022**, *12*, 10662. [CrossRef]
27. Pham, T.D.; Xia, J.S.; Ha, N.T.; Bui, D.T.; Le, N.N.; Tekeuchi, W. A Review of Remote Sensing Approaches for Monitoring Blue Carbon Ecosystems: Mangroves, Seagrassesand Salt Marshes during 2010–2018. *Sensors* **2019**, *19*, 1933. [CrossRef]
28. Wang, H.J.; Xia, C.; Liu, X.P.; Zhang, A.Q.; Zhu, Y.R.; Wang, H.X. Theoretical and Methodological Perspectives of Fine-Scale Urban Expansion Cellular Automata for the Large Regions. *Geogr. Geoinf. Sci.* **2016**, *32*, 1–8. [CrossRef]
29. Clarke, K.C.; Gaydos, L.J. Loose-coupling a cellular automaton model and GIS: Long-term urban growth prediction for San Francisco and Washington/Baltimore. *Int. J. Geogr. Inf. Sci.* **1998**, *12*, 699–714. [CrossRef]
30. Luan, C.X.; Liu, R.Z. A Comparative Study of Various Land Use and Land Cover Change Models to Predict Ecosystem Service Value. *Int. J. Environ. Res. Public Health* **2022**, *19*, 16484. [CrossRef]
31. Wang, F.; Marceau, D.J. A Patch-based Cellular Automaton for Simulating Land-use Changes at Fine Spatial Resolution. *T. GIS* **2013**, *17*, 828–846. [CrossRef]
32. Chen, Y.M.; Li, X.; Liu, X.P.; Ai, B.; Li, S.Y. Capturing the varying effects of driving forces over time for the simulation of urban growth by using survival analysis and cellular automata. *Landsc. Urban Plan.* **2016**, *152*, 59–71. [CrossRef]
33. Liang, X.; Liu, X.P.; Li, D.; Zhao, H.; Chen, G.Z. Urban growth simulation by incorporating planning policies into a CA-based future land-use simulation model. *Int. J. Geogr. Inf. Sci.* **2018**, *32*, 2294–2316. [CrossRef]
34. Lin, J.Y.; Li, X.; Wen, Y.Y.; He, P.T. Modeling urban land-use changes using a landscape-driven patch-based cellular automaton (LP-CA). *Cities* **2023**, *132*, 103906. [CrossRef]

35. Liang, X.; Guan, Q.F.; Clarke, K.C.; Liu, S.S.; Wang, B.Y.; Yao, Y. Understanding the drivers of sustainable land expansion using a patch-generating land use simulation (PLUS) model: A case study in Wuhan, China. *Comput. Environ. Urban Syst.* **2021**, *85*, 101569. [CrossRef]
36. Wang, Z.Y.; Huang, C.L.; Li, L.; Lin, J. Ecological zoning planning and dynamic evaluation coupled with Invest-HFI-Plus model: A case study in Bortala Mongolian Autonomous Prefecture. *Acta Ecol. Sin.* **2022**, *42*, 5789–5798. [CrossRef]
37. Li, C.; Wu, Y.M.; Gao, B.P.; Zheng, K.J.; Wu, Y.; Li, C. Multi-scenario simulation of ecosystem service value for optimization of land use in the Sichuan-Yunnan ecological barrier, China. *Ecol. Indic.* **2021**, *132*, 108328–108341. [CrossRef]
38. Liang, X.; Liu, X.P.; Li, X.; Chen, Y.M.; Tian, H.; Yao, Y. Delineating multi-scenario urban growth boundaries with a CA-based FLUS model and morphological method. *Landsc. Urban Plan.* **2018**, *177*, 47–63. [CrossRef]
39. Liu, X.P.; Liang, X.; Li, X.; Xu, X.C.; Ou, J.P.; Chen, Y.M.; Li, S.Y.; Wang, S.J.; Pei, F.S. A future land use simulation model (FLUS) for simulating multiple land use scenarios by coupling human and natural effects. *Landsc. Urban Plan.* **2017**, *168*, 94–116. [CrossRef]
40. Ghosh, P.; Mukhopadhyay, A.; Chanda, A.; Mondal, P.; Akhand, A.; Mukherjee, S.; Nayak, S.K.; Ghosh, S.; Mitra, D.; Ghosh, T.; et al. Application of Cellular automata and Markov-chain model in geospatial environmental modeling—A review. *Remote Sens. Appl. Soc. Environ.* **2017**, *5*, 64–77. [CrossRef]
41. Jenerette, G.D.; Harlan, S.L.; Buyantuev, A.; Stefanov, W.L.; Declet-Barreto, J.; Ruddell, B.L.; Myint, S.W.; Kaplan, S.; Li, X.X. Micro-scale urban surface temperatures are related to land-cover features and residential heat related health impacts in Phoenix, AZ USA. *Landsc. Ecol.* **2016**, *31*, 745–760. [CrossRef]
42. Pandey, K.; Mitra, D.; Maithani, S.; Karnatak, H. Urban Growth Modelling Using Cellular Automata—Markov (CA-Markov) Technique. *J. Appl. Math. Comput.* **2018**, *2*, 178–187. [CrossRef]
43. Sun, D.Z.; Liang, Y.J. Multi-scenario simulation of land use dynamic in the Loess Plateau using an improved Markov-CA model. *J. Geoinf. Sci.* **2021**, *23*, 825–836. [CrossRef]
44. Lang, Y.Q.; Song, W. Quantifying and mapping the responses of selected ecosystem services to projected land use changes. *Ecol. Indic.* **2019**, *102*, 186–198. [CrossRef]
45. Jiang, H.L.; Xu, X.; Guan, X.; Wang, L.F.; Huang, Y.M.; Liu, Y.H. Simulation of Spatiotemporal Land Use Changes for Integrated Model of Socioeconomic and Ecological Processes in China. *Sustainability* **2019**, *11*, 3627. [CrossRef]
46. Fan, Z.M. Simulation of land-cover change in Jing-Jin-Ji region under different scenarios of SSP-RCP. *J. Geogr. Sci.* **2022**, *32*, 421–440. [CrossRef]
47. Su, B.D.; Huang, J.L.; Mondal, S.K.; Zhai, J.Q.; Wang, Y.J.; Wen, S.S.; Gao, M.N.; Lv, Y.R.; Jiang, S.; Jiang, T.; et al. Insight from CMIP6 SSP-RCP scenarios for future drought characteristics in China. *Atmos. Res.* **2021**, *250*, 105375–105393. [CrossRef]
48. Zhao, X.; Zhu, M.Y.; Liu, D.D.; Xu, S.Q.; Ye, S.Y.; Wang, S.; Cui, Y.P.; Zhou, S.H. Exploring the Ecological Climate Effects of Different Land Use Changes in the Yangtze River Basin from 2000 to 2020. *Land* **2022**, *11*, 1636. [CrossRef]
49. Li, J.; Chunyu, X.Z.; Huang, F. Land Use Pattern Changes and the Driving Forces in the Shiyang River Basin from 2000 to 2018. *Sustainability* **2022**, *15*, 154. [CrossRef]
50. Xu, D.H.; Zhang, K.; Cao, L.H.; Guan, X.R.; Zhang, H.B. Driving forces and prediction of urban land use change based on the geodetector and CA-Markov model: A case study of Zhengzhou, China. *Int. J. Digit. Earth* **2022**, *15*, 2246–2267. [CrossRef]
51. Zhu, H.X.; Ou, X.J.; Yang, Z.; Yang, Y.W.; Ren, H.X.; Tang, L. Spatiotemporal Dynamics and Driving Forces of Land Urbanization in the Yangtze River Delta Urban Agglomeration. *Land* **2022**, *11*, 1365. [CrossRef]
52. Mohammad, A.; Ali, A.A.; Raid, S.; Babikir, M. Land Use Land Cover Change Analysis for Urban Growth Prediction Using Landsat Satellite Data and Markov Chain Model for Al Baha Region Saudi Arabia. *Forests* **2022**, *13*, 1530. [CrossRef]
53. Hurtt, G.C.; Chini, L.; Sahajpal, R.; Frolking, S.; Bodirsky, B.L.; Calvin, K.; Doelman, J.C.; Fisk, J.; Fujimori, S.; Goldewijk, K.K.; et al. Harmonization of global land use change and management for the period 850–2100 (LUH2) for CMIP6. *Geosci. Model Dev.* **2020**, *13*, 5425–5464. [CrossRef]
54. Chen, L.J.; Liu, G.H.; Li, H.G. Estimating Net Primary Productivity of Terrestrial Vegetation in China Using Remote Sensing. *J. Remote Sens.* **2002**, *6*, 129–135+164.
55. Xie, X.L.; Sun, B.; Zhou, H.Z.; Li, Z.P.; Li, A.B. Organic Carbon Density and Storage in soils of China and Spatial Analysis. *Acta Pedol. Sin.* **2004**, *41*, 35–43.
56. Li, K.R.; Wang, S.Q.; Cao, M.K. Vegetation and Soil Carbon Storage in China. *Sci. China Ser. D* **2003**, *01*, 72–80. [CrossRef]
57. Li, L.; Fu, W.; Luo, M.C. Spatial and Temporal Variation and Prediction of Ecosystem Carbon Stocks in Yunnan Province Based on Land Use Change. *Int. J. Environ. Res. Public Health* **2022**, *19*, 16059. [CrossRef]
58. Li, X.; Chen, G.Z.; Liu, X.P.; Liang, X.; Wang, S.J.; Chen, Y.M.; Pei, F.S.; Xu, X.C. A New Global Land-Use and Land-Cover Change Product at a 1-km Resolution for 2010 to 2100 Based on Human–Environment Interactions. *Ann. Am. Assoc. Geogr.* **2017**, *107*, 1303357. [CrossRef]
59. Schaldach, R.; Alcamo, J.; Koch, J.; Kölking, C.; Lapola, D.M.; Schüngel, J.; Priess, J.A. An integrated approach to modelling land-use change on continental and global scales. *Environ. Model. Softw.* **2011**, *26*, 1041–1051. [CrossRef]
60. Tubiello, F.N.; Salvatore, M.; Ferrara, A.F.; House, J.; Federici, S.; Rossi, S.; Biancalani, R.; Condor, G.R.D.; Jacobs, H.; Flammini, A.; et al. The Contribution of Agriculture, Forestry and other Land Use activities to Global Warming, 1990–2012. *Glob. Change Biol.* **2015**, *21*, 2655–2660. [CrossRef]
61. Hergoualc'h, K.; Verchot, L.V. Greenhouse gas emission factors for land use and land-use change in Southeast Asian peatlands. *Mitig. Adapt. Strateg. Glob. Change* **2014**, *19*, 789–807. [CrossRef]

62. Houghton, R.A. Aboveground Forest Biomass and the Global Carbon Balance. *Glob. Change Biol.* **2005**, *11*, 945–958. [CrossRef]
63. Luo, Y.Q.; Niu, S.L. Mature forest shows little increase in carbon uptake in a CO2-enriched atmosphere. *Nature* **2020**, *580*, 191–192. [CrossRef] [PubMed]
64. Wang, H.H.; Yue, C.; Mao, Q.Q.; Zhao, J.; Ciais, P.; Li, W.; Yu, Q.; Mu, X.M. Vegetation and species impacts on soil organic carbon sequestration following ecological restoration over the Loess Plateau, China. *Geoderma* **2020**, *371*, 114389. [CrossRef]
65. Chen, W.X.; Zhao, H.B.; Li, J.F.; Zhu, L.J.; Wang, Z.Y.; Zeng, J. Land use transitions and the associated impacts on ecosystem services in the Middle Reaches of the Yangtze River Economic Belt in China based on the geo-informatic Tupu method. *Sci. Total Environ.* **2020**, *701*, 134690. [CrossRef]
66. Qiao, W.Y.; Guan, W.H.; Huang, X.J. Assessing the Potential Impact of Land Use on Carbon Storage Driven by Economic Growth: A Case Study in Yangtze River Delta Urban Agglomeration. *Int. J. Environ. Res. Public Health* **2021**, *18*, 11924. [CrossRef]
67. Chen, J.D.; Xu, C.; Wang, Y.Z.; Li, D.; Song, M.L. Carbon neutrality based on vegetation carbon sequestration for China's cities and counties: Trend, inequality and driver. *Resour. Policy* **2021**, *74*, 102116–102403. [CrossRef]
68. Zhao, Y.; Zhong, L.; Ma, Y.M.; Fu, Y.F.; Chen, M.X.; Ma, W.Q.; Zhao, C.; Huang, Z.Y.; Zhou, K.Q. WRF/UCM simulations of the impacts of urban expansion and future climate change on atmospheric thermal environment in a Chinese megacity. *Clim. Change* **2021**, *169*, 38. [CrossRef]
69. Ren, H.Q.; Cai, G.Y.; Zhao, G.Q.; Li, Z.Q. Accuracy Assessment of the GlobeLand30 Dataset in Jiangxi Province. *Int. Arch. Photogramm. Remote Sens. Spatial Inf. Sci.* **2018**, *XLII-3*, 1481–1487. [CrossRef]
70. He, C.; Zhang, J.X.; Wan, Y.; Yang, W.J.; Yang, R.N. Accuracy Assessment of GlobeLand30 2020 Based on Spatial Sampling: A Case Study in Shanghai. *Geospat. Inf.* **2022**, *20*, 93–96+106.
71. Wang, Z.X.; Xing, H.F.; Zhang, H.X.; Shu, Y.Q.; Meng, Y.; Li, B. Employing Crowdsourced Geographic Information for GlobeLand30 Artificial Surface Validation. *Geomat. World* **2021**, *28*, 100–105.